

Energy & Environmental Science

Accepted Manuscript



This is an *Accepted Manuscript*, which has been through the Royal Society of Chemistry peer review process and has been accepted for publication.

Accepted Manuscripts are published online shortly after acceptance, before technical editing, formatting and proof reading. Using this free service, authors can make their results available to the community, in citable form, before we publish the edited article. We will replace this *Accepted Manuscript* with the edited and formatted *Advance Article* as soon as it is available.

You can find more information about *Accepted Manuscripts* in the [Information for Authors](#).

Please note that technical editing may introduce minor changes to the text and/or graphics, which may alter content. The journal's standard [Terms & Conditions](#) and the [Ethical guidelines](#) still apply. In no event shall the Royal Society of Chemistry be held responsible for any errors or omissions in this *Accepted Manuscript* or any consequences arising from the use of any information it contains.



Journal Name

ARTICLE

Capture of iodine and organic iodides using silica zeolites and the semiconductor behaviour of iodine in a silica zeolite

Received 00th September 2015,
Accepted 00th September 2015

DOI: 10.1039/x0xx00000x

www.rsc.org/

Tung Cao Thanh Pham,^a Son Docao,^a In Chul Hwang,^a Mee Kyung Song,^a Do Young Choi,^a
Dohyun Moon,^b Peter Oleynikov^c, Kyung Byung Yoon^{a,*}

During the reprocessing of spent nuclear fuel rods, a highly moist off-gas mixture containing various volatile radioactive species such as iodine (I₂), organic iodides and nitric acid, is produced. Efforts have been made to devise materials, which can effectively capture radioactive iodine (I₂) and organic iodides from the off-gas without being damaged by moisture, nitric acid, and I₂. In the investigation described herein, we observed that all-silica zeolites, such as silicalite-1 and Si-BEA, are stable in 5 M nitric acid and adsorb I₂, CH₃I, and CH₃CH₂I from highly acidic off-gas mixtures to much greater extents than does activated carbon. In particular, the hydrophobicity-intensified silicalite-1 performs best. We further found that I₂ forms a unique semiconducting three-dimensional supramolecular network within the silicalite-1 channels. The conductivity of the fully I₂ loaded silicalite-1 is observed to be ca. 10⁴ S m⁻¹, which is ca. 10⁸-fold higher than that of solid I₂.

Broad Context

To reduce the greenhouse gas concentration in the atmosphere, the utilization of nuclear energy is receiving more attention than ever. Currently, about 435 nuclear reactors are under operation worldwide and more than 70 nuclear reactors are newly being built. For their proper operation the spent nuclear fuel rods should be reprocessed safely. The reprocessing of spent fuel rods starts with dissolving them in hot highly concentrated (3-5 M) nitric acid. During this step the off-gas mixture consisting of radioactive iodine (I₂) and alkyl iodides (RI) and other volatile radioactive species are produced. The off-gas mixture also contains nitric acid vapor and NO_x as well as moisture. Accordingly, the off-gas mixture is highly radioactive, highly acidic, highly oxidizing, and humid. Therefore, the I₂- and RI-capturing materials should be stable and have high affinities to I₂ and RI under such a harsh off-gas mixture condition. The materials should also be capable of directly capturing them even from the highly acidic and highly radioactive dissolver solution. If possible, the I₂- and RI-capturing materials should be recycled to minimize the volume of the radioactive wastes to be discarded. This work demonstrates that all silica zeolites, in particular hydrophobicity-intensified silicalite-1, perform best among various tested materials.

Introduction

Despite their potentially hazardous nature, nuclear power

plants have an increasing worldwide demand. Under normal operating conditions, spent nuclear fuel rods used for energy generation in these plants need to be reprocessed. The first step in the reprocessing sequence involves dissolving the spent rods in hot concentrated nitric acid¹⁻³. During dissolution and in subsequent steps in the sequence, highly radioactive, acidic, reactive and moist off-gases, consisting of nitric acid, NO₂, and N₂O₅, along with radioactive molecular iodine (I₂) and alkyl iodides (RI) (e. g., methyl iodide (CH₃I)

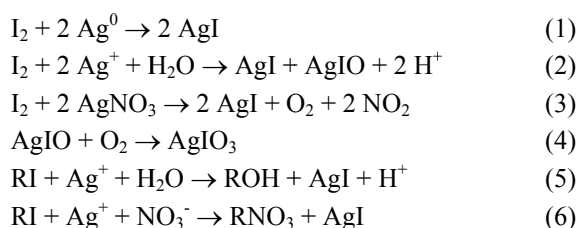
^a Center for Nanomaterials, Korea Center for Artificial Photosynthesis, Department of Chemistry, Sogang University, Seoul 121-742, Korea

^b Supramolecule/Small molecule Crystallography, Pohang Accelerator Laboratory, San 31 Hyoja-Dong, Nam-Gu, Pohang, KyungBuk, 790-784, Korea.

^c Department Materials and Environmental Chemistry, Stockholm University, SE-106 91 Stockholm, Sweden.

*Electronic Supplementary Information (ESI) available: [details of any supplementary information available. See DOI: 10.1039/x0xx00000x]

and ethyl iodide ($\text{CH}_3\text{CH}_2\text{I}$) are produced. Radioactive (I_2) and alkyl iodides (RI) in the off-gas mixture must be selectively captured and sequestered¹⁻³. The procedures employed for this purpose can be classified into liquid-phase methods and solid sorbents-based fixed bed methods, the latter of which have proven to be more economical¹⁻³. The active components of the solid sorbent mixtures used in fixed bed methods are silver nanoparticles (Ag^0), silver ion (Ag^+) or silver nitrate (AgNO_3), which are supported on various solid supports including silica, alumina, zeolites, and activated carbon (denoted as AC)¹⁻⁷. The silver species capture radioactive I_2 and RI by promoting their conversion to water insoluble AgI or AgIO_3 through the reactions displayed in Eqs 1-6⁷.



The temperature of the off-gas is usually ca. 150 °C in order to accelerate the chemical reactions and remove adsorbed water from the narrow pores of the support¹⁻⁷. The AgI/AgIO_3 containing solid sorbents are typically removed from the fixed bed column and then vitrified for permanent sequestration. Two important disadvantages of Ag-based sorbents are that only a portion of silver species participates in the I_2 and RI capturing processes¹⁻³, and that all of the spent solid sorbents need to be discarded.

AgI and AgIO_3 in the spent adsorbents can be converted back to Ag^0 nanoparticles by treatment with molecular hydrogen at high temperatures (ca. 500 °C). During this process, radioactive HI vapour is produced, which is trapped by using an AgNO_3 solution¹⁻³. However, the regenerated Ag nanoparticles undergo gradual sintering during the regeneration process, which leads to a significant decrease in their activity. Because of this deleterious feature, the expensive adsorbents are typically discarded after being recycled several times¹⁻³.

Removal of I_2 and RI from off-gas mixtures would be much simpler and economical if the solid sorbents used in the process were both abundantly available and cheap, and if the

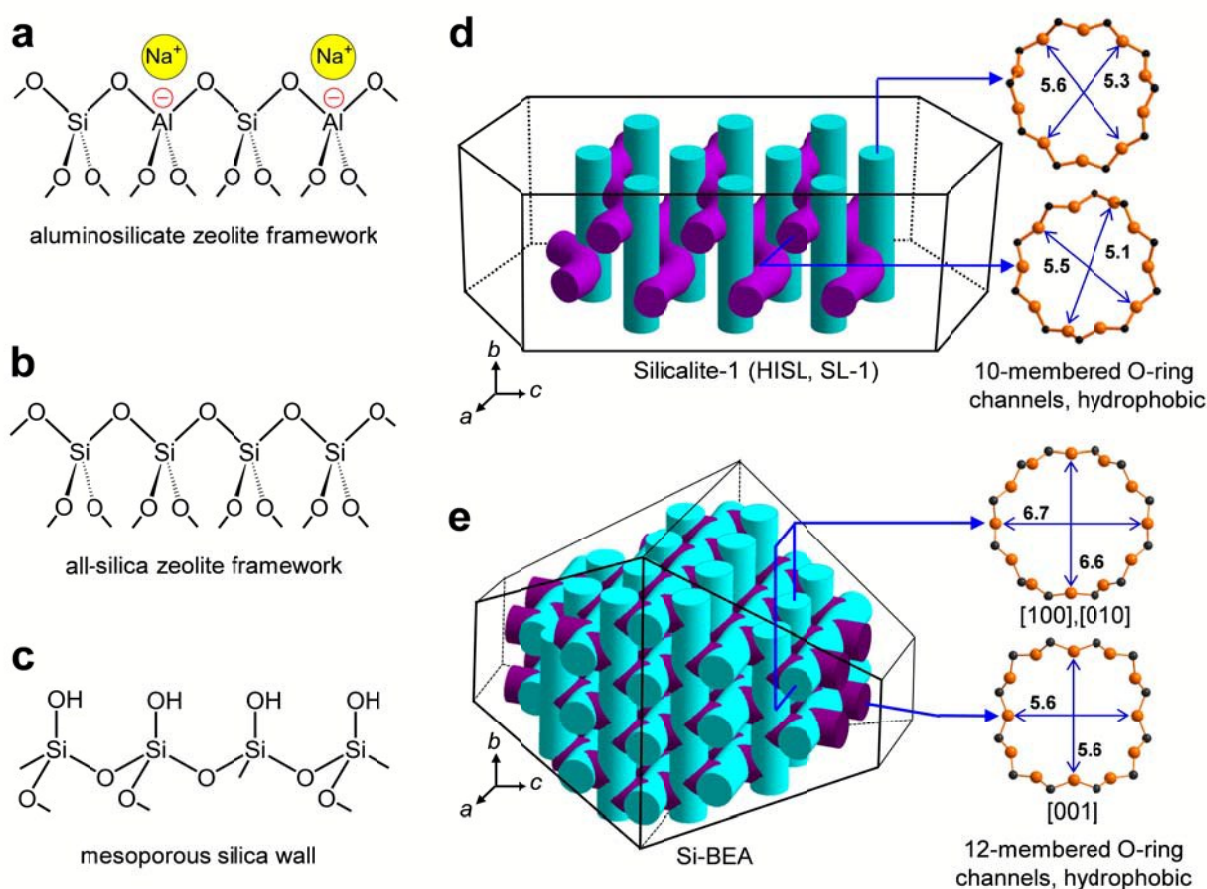


Fig. 1. Typical framework structures of aluminosilicate zeolites (a), all-silica zeolites (b), and mesoporous silica (c). Typical morphology, the channel arrangements, and channel opening sizes of silicalite-1 (SL-1) and hydrophobicity-intensified silicalite-1 (HISL) (d) and all-silica BEA (Si-BEA) (e)

regeneration cycle were more operationally simple and if it occurred at moderate temperatures. Consequently, it would be ideal if physical sorbents could be employed in place of Ag-based chemical sorbents. Moreover, the physical sorbents would need to be hydrophobic in order to be able to adsorb I₂ and RI under highly humid conditions, to be resistant to oxidation by I₂ and nitric acid, and to be stable under highly acidic conditions. Owing to these restrictions, aluminosilicate zeolites are not suitable sorbents because they are hydrophilic by nature caused by the presence of negative charges and charge balancing cations (Fig. 1a). In addition, negatively charged aluminosilicate zeolites frameworks are basic and, hence, they readily decompose in acidic media. Finally, these frameworks are readily oxidatively decomposed by molecular iodine⁸ leading to the formation of I⁻ (or I₃⁻). Importantly, all-silica zeolites with the framework structure shown in Fig. 1b would be ideal physical sorbents for removal of I₂ and RI because they are hydrophobic and resistant to acid and oxidizing agents. The related mesoporous silica materials are not suitable for this purpose because their pore interiors are covered with hydroxyl groups (Fig. 1c) which make the pores hydrophilic.

Metal organic frameworks (MOFs) such as ZIF-8, HKUST-1, and others have also been tested as I₂-capturing materials⁹⁻¹³. However, their electron-rich organic ligands readily reduce I₂ in aqueous solutions to form I⁻ (see below). Furthermore, the MOFs are not stable in acidic environments. Moreover, HKUST-1 is extremely hydrophilic and, as a result, it cannot be employed as a physical sorbent for I₂ in a humid atmosphere or an aqueous solution. AC has also been widely tested as a physical I₂ sorbent^{3,6} and as a support for Ag¹⁻³. However, this material ignites in the presence of hot NO₂ gas¹⁻³, and it contains various electron-rich organic functional groups, which readily reduce I₂. In this light, MOFs can be viewed as organic salts and, hence, they also have the potential to ignite in the presence of hot NO₂ gas.

Based on the information provided above, we designed a study to explore the potential use of typical all-silica zeolites, such as silicalite-1 (denoted as SL-1, Fig. 1d) and all-silica BEA (Si-BEA, Fig. 1e), as a physical sorbent for I₂ and RI. In this effort, we evaluated the I₂ and RI adsorption capacities of these materials as well as their inertness towards I₂. AC, Na⁺-exchanged zeolite X (NaX), Na⁺-exchanged zeolite Y (NaY), Na⁺-exchanged zeolite A (NaA), Ca²⁺-exchanged zeolite A (CaA), Na⁺-exchanged mordenite (NaM), Ag⁺-exchanged mordenite (AgM), and Ag⁰-containing mordenite (Ag⁰M), Na⁺-exchanged ZSM-5 (NaZSM-5), SBA-15, ZIF-8¹⁴, HKUST-1¹⁵, and zinc saccharate (ZnSacc)¹⁶ were also employed as physical I₂ sorbents in order to compare their results with those of SL-1 and Si-BEA. ZnSacc is a three-dimensional coordination polymer consisting of D-saccharate and Zn²⁺¹⁶, which possesses both hydrophilic and

hydrophobic channels and adsorbs I₂ vapor (16.6% at 19 °C after adsorption for 5 d)¹⁶. ZSM-5 is isostructural with SL-1 and it has a aluminosilicate framework with a relatively high Si/Al ratio (>25) that differentiates it from Al-richer aluminosilicate zeolites (zeolites A, X, and Y, with Si/Al ratios <3).

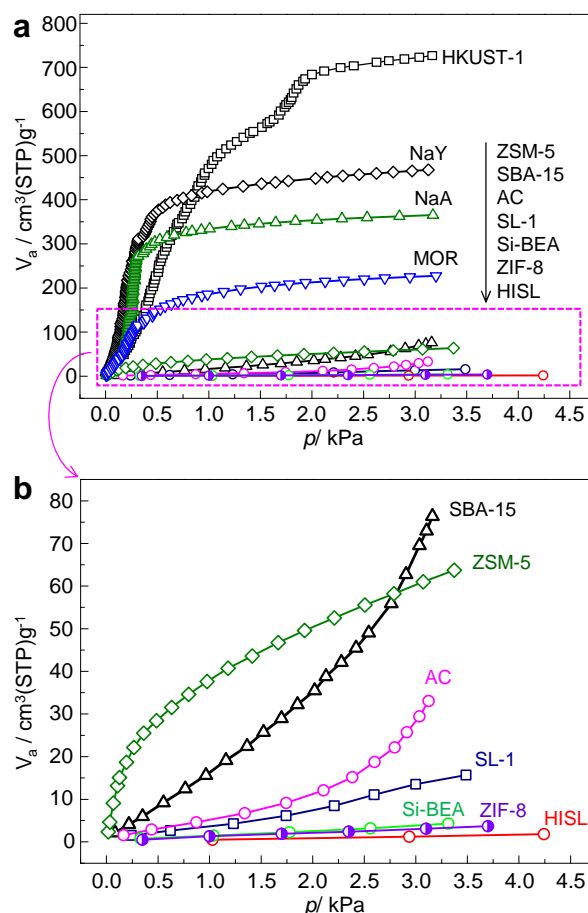


Fig. 2. Water adsorption isotherms of various adsorbents as indicated. The isotherms of all adsorbents (a) and the enlarged isotherms of the hydrophobic adsorbents (b). This result indicates that HISL is most hydrophobic and HKUST-1 is least hydrophobic.

SL-1 has $5.5 \times 5.1 \text{ \AA}$ sized channels aligned in a sinusoidal manner along the *a* axis (denoted as *a*-channels) and $5.6 \times 5.3 \text{ \AA}$ sized channels arranged linearly along the *b* axis (denoted as *b*-channels) (Fig. 1d). The crystal density of SL-1 is 1.796 Mg/m^3 . The porosity $\{[(\text{pore volume in a unit cell})/(\text{unit cell volume})] \times 100, \text{ in \%}\}$ of SL-1 is 29.2%. Although SL-1 is an all-silica zeolite, it still displays a low level of hydrophilicity owing to framework defects. However, it is known that the number of defects and hence hydrophilicity significantly decreases when SL-1 is synthesized in a gel containing a F⁻-liberating reagent¹⁷. Therefore, in this study we prepared less defected and more

hydrophobic or hydrophobicity-intensified SL-1 (denoted as HISL) using the method described in Methods and tested its I_2 and RI adsorbing properties.

Si-BEA has $6.7 \times 6.6 \text{ \AA}$ sized straight channels running along the a and b axes and the a - and b -channels slightly cross creating a $5.6 \times 5.6 \text{ \AA}$ sized interfacial opening at each channel cross section (Fig. 1e).¹⁸ The crystal density of Si-BEA is 1.5281 Mg/m^3 , which is smaller than that of SL-1, indicating that Si-BEA is more porous than SL-1. Indeed, the porosity of Si-BEA is 35.6%, which is larger than that of SL-1 by 22%.

In this investigation, we observed that HISL, SL-1, Si-BEA display unique properties in terms of their chemical resistance to I_2 and 5 M nitric acid, their high capturing capacities for I_2 , CH_3I , and CH_3CH_2I from the moist Ar streams under simulated off-gas conditions, and their high I_2 capturing capacity under a simulated dissolver solution conditions. In an extension of this effort, we elucidated the crystal structure of 12 I_2 -incorporated HISL ($12I_2@HISL$), determined its total energy and electronic properties by using first-principles calculations with CASTEP, and finally uncovered its interesting semiconductor property.

Results and discussion

Extremely hydrophobic HISL

The water adsorption profiles of various materials are shown in Fig. 2. Based on the total amounts of adsorbed water the order of hydrophobicity can be deduced as $HISL < ZIF-8 \approx Si-BEA < SL-1 < AC < NaZSM-5 < SBA-15 < NaM < NaA < NaY < HKUST-1$. This result shows that all-silica zeolites are more hydrophobic than AC, HISL is most hydrophobic among the tested materials, and the hydrophobicity intensification of SL-1 by decreasing the number of defect site in SL-1 really works well. Interestingly Si-BEA is slightly less hydrophobic than HISL despite the fact that both gels for HISL and Si-BEA commonly contain $(NH_4)_2SiF_6$ as the F^- source. ZIF-8 is also slightly less hydrophobic than HISL but decomposes in the acidic environment. AC is also hydrophobic from the general point of view but much less hydrophobic than all-silica zeolites. HKUST-1 is least hydrophobic or most hydrophilic. It also decomposes in the acidic environment, and hence is not suitable as the material to capture I_2 from the humid and acidic stream of off-gas.

Capturing capacities of HISL for I_2 , CH_3I , and CH_3CH_2I

I_2 capturing capacities were determined by passing streams of a dry gas mixture containing I_2 and Ar at room temperature through columns charged with HISL, SL-1, Si-BEA, AC, HKUST-1, Zn-Sacc, and ZIF-8 for 15 h. The results show that the respective amounts of I_2 captured under these

conditions are 0.53, 0.48, 0.47, 0.70, 0.38, 0.05, and 0.03 g per gram of each sorbent (Fig. 3a). The amount of I_2 captured by SL-1 is smaller than that of HISL by 9%. The increase in hydrophilicity and the partial blocking of the channels induced by defect sites are ascribed as the reason for this phenomenon. In the case of Si-BEA, the decrease in the captured amount of I_2 with respect to that of HISL is 11%, despite the fact that the porosity of Si-BEA is larger than that of HISL by 22% while its hydrophobicity is only slightly less than that of HISL. We therefore ascribe the 'less tight fit' of I_2 molecules within the larger (wider) channels of Si-BEA than in smaller channels in HISL as the main reason to the decrease in the captured amount of I_2 on going from HISL to Si-BEA. We found that c.a. 13% of the amount of I_2 captured by AC exists in the form of iodide (I^-), generated through a redox reaction promoted by functional groups in AC. All of the I_2 captured by HKUST-1, Zn-Sacc, and ZIF-8 exists in the form of I^- .

In cases of HISL, Si-BEA, and AC we further explored the I_2 capturing abilities under the humid and simulated acidic off gas conditions, created by passing a dry stream consisting of I_2 vapour and Ar into the 5 M nitric acid (HNO_3) solution. The I_2 capturing abilities of HISL, Si-BEA, and AC were observed to remain high even when a humid off gas mixture is employed (Fig. 3b). Although the amount of I_2 (in grams) captured by AC in terms of gram of I_2 per gram of host (g/g) is higher than those of HISL, the amount (in grams) per mL captured by AC is much lower than those of HISL and Si-BEA (Fig. 3c). This phenomenon arises from the fact that the bulk densities of $1 \mu\text{m}$ size HISL and $3\text{-}4 \mu\text{m}$ size Si-BEA used in this study (0.87 and 0.83 g/mL , respectively) are much higher than that of AC (0.313 g/mL). This result shows that HISL is the most suitable I_2 capturing material owing to the fact that a capturing column with the smallest volume can be employed.

The respective amounts of I_2 captured by HISL, Si-BEA, and AC under simulated acidic off gas conditions are 0.30, 0.26, and 0.12 g/g or 0.26, 0.21, and 0.04 g/mL (Fig. 3d,e). While I_2 captures by HISL and Si-BEA are 43% lower under simulated acidic off gas conditions as compared to humid nonacidic conditions, capture by AC is lowered by 83% as a consequence of this change. As a result, the I_2 capturing ability of HISL under simulated acidic off gas conditions exceeds that of AC by more than two times in terms of g/g and more than six times in terms of g/mL. Furthermore, the I_2 removal efficiency [$1 - (C_{out}/C_{in})$, where C_{out} = concentration of I_2 at the outlet, C_{in} = concentration of I_2 in the inlet] is 1 during the period of I_2 adsorption when the packed HISL is not saturated with I_2 (Fig. 4). In fact, the amounts of I_2 captured by HISL at room temperature under dry and humid conditions are higher than those using Ag-exchanged

aluminosilicate zeolites at 150 °C (0.53 g/g vs. 0.08-0.20 g/g adsorbed)¹⁻³. Moreover, the I₂ solubility in HISL is as much as 94.8 g/100 mL from the single crystal point of view, which is much higher than those of organic solvents (1-25 g/100 mL) and water (0.03 g/100 mL). The amount of I₂ adsorbed per 100 mL of HISL powder is 46.0 g, a value that is much larger than that of AC powder (22.0 g/100 mL). Thus, the observations show that HISL and Si-BEA are excellent sorbents for I₂ from a room temperature stream of I₂ vapor under simulated acidic off gas conditions. In particular, HISL is the best I₂ sorbent under this condition.

The results of further studies demonstrate that HISL readily adsorbs large amounts of methyl iodide (CH₃I) and ethyl iodide (CH₃CH₂I) from respective streams consisting of CH₃I and Ar, and CH₃CH₂I and Ar under dry, humid, and simulated off-gas conditions. The respective amounts of CH₃I and CH₃CH₂I captured under the dry and humid conditions

(CH₃I = 0.42 g/g or 0.37 g/mL, CH₃CH₂I = 0.26 g/g or 0.23 g/mL) (Fig. 3f,g) are 17 and 10 molecules per unit cell of HISL. Because the estimated molecular lengths of I₂, CH₃I, and CH₃CH₂I are 6.66, 5.10, and 6.68 Å, respectively, incorporation of a larger number of CH₃I molecules into the HISL unit cell as compared to those of CH₃CH₂I and I₂ is reasonable. Under the simulated off-gas condition, the captured amounts decreased to 0.36 g/g of CH₃I and 0.25 g/g of CH₃CH₂I. In comparison, the captured amounts by Si-BEA and AC under the simulated off-gas condition were slightly lower, 0.34 and 0.34 g/g of CH₃I and 0.22 and 0.21 g/g of CH₃CH₂I, respectively. As expected, HISL does not adsorb hydrogen iodide HI, a polar molecule, despite the fact that it is also an important radioactive species that requires capture and sequestration. The combined results of this investigation show that HISL is a highly effective adsorbent of I₂ vapour, CH₃I and CH₃CH₂I from humid, highly acidic and oxidizing

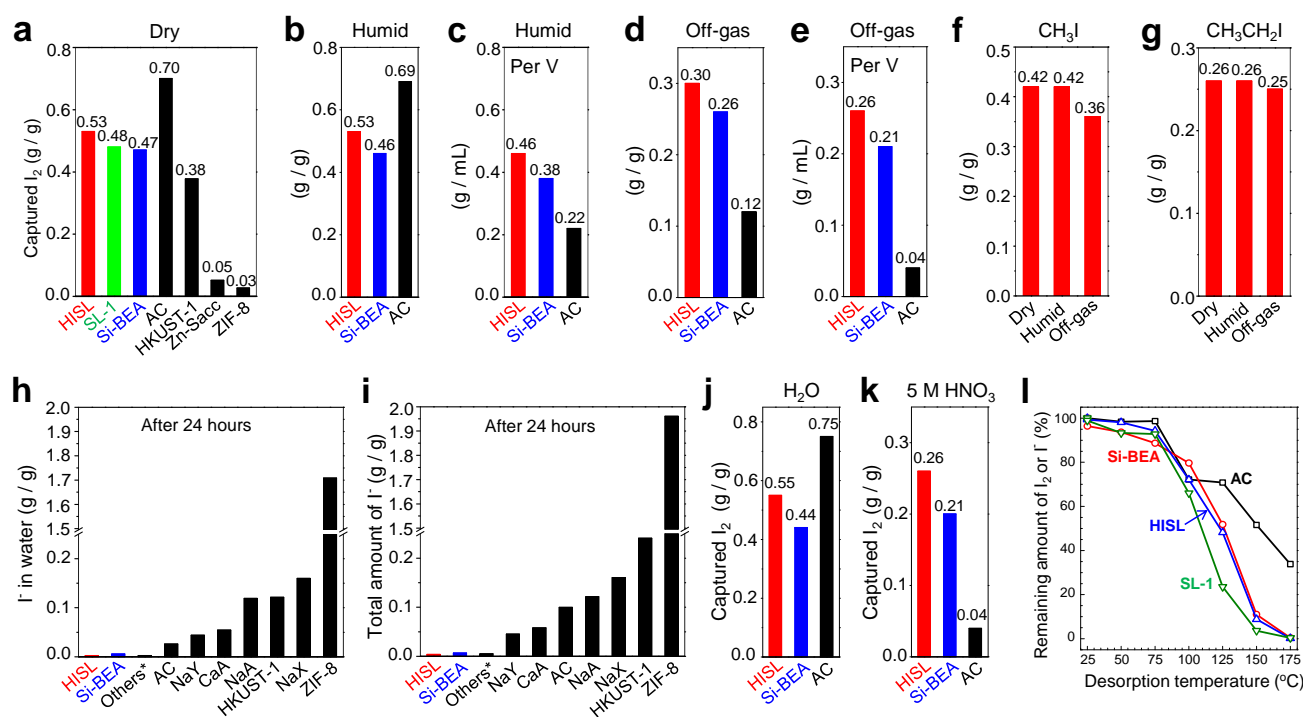


Fig. 3. Bar graphs of the captured amounts of I₂ from the dry stream of I₂ vapor and Ar at room temperature for the host materials indicated below (a), captured amounts of I₂ by HISL, Si-BEA, and AC from the humid stream of I₂ vapor and Ar at room temperature per gram (b) and per mL (c) of each host, captured amounts of I₂ at room temperature by HISL, Si-BEA, and AC from a simulated acidic off-gas consisting of I₂ vapor, HNO₃ vapor and its decomposed products, and Ar per gram (d) and per mL (e) of each host, captured amounts of CH₃I (f) and CH₃CH₂I (g) by HISL from the streams of CH₃I and CH₃CH₂I, respectively, diluted by Ar under the dry, humid, and off-gas conditions, the amounts of iodide (I⁻) produced in the solution (h) and the total amounts existing both in the solution and within the material (i) by the materials indicated below upon immersion into the aqueous solution of I₂ for 24 h, the captured amounts of I₂ by HISL, Si-BEA, and AC from a neutral aqueous solution (j) and 5 M HNO₃ solution (k) dissolved with I₂, and the temperature dependent desorption profiles of fully I₂-incorporated HISL, SL-1, Si-BEA, and AC in the temperature region between 25 and 175 °C (l). Others* in panels h and i are SL-1, NaZSM-5, Ag⁰M, AgM, NaM, and SBA-15.

off gas mixtures.

Although most I_2 produced in the dissolver solution during the capturing process is transmitted into the dissolver off-gas, some of this substance remains in the dissolver solution. In order to remove residual amounts of I_2 from this solution, a capturing material can be added. However, the material employed for this purpose should satisfy the following requirements. Firstly, the material should resist oxidation by I_2 , a property that can be judged by quantitative analysis of the amount of iodide (I^-) formed in the solution after addition of the material. The results of our studies show that HISL, Si-BEA, and other electron poor materials such as SL-1, NaZSM-5, AgM, NaM, SBA-15 do not promote production of iodide (I^-) when added to I_2 containing solutions (Fig. 3h).

In contrast, electron rich materials such as ZIF-8, HKUST-1, NaX, NaA, AC, CaA, and NaY induce the formation of varying amounts of iodide in the solution (Fig. 3h). As a result, these materials are not suitable for use in the removal of I_2 from the dissolver solution. In particular, highly electron rich ZIF-8 promotes production of a large amount of I^- (1.96 g/g) in an aqueous solution after 24 h, caused by $2e^-$ oxidation by I_2 of its highly electron-rich methyl imidazolate moieties. HKUST-1 also decomposes in the presence of I_2 . AC, ZIF-8, and ZnSacc promote formation of I^- which is retained in small amounts within their structures.

The comparison of the total amount of I^- existing both in solution and in the adsorbent after 24 h is shown for each of these sorbents in Fig. 3i. Interestingly, a relationship was found to exist between the Sanderson's partial negative

charge of oxygen ($-\delta_o$)¹⁹ of the zeolites and the total amount

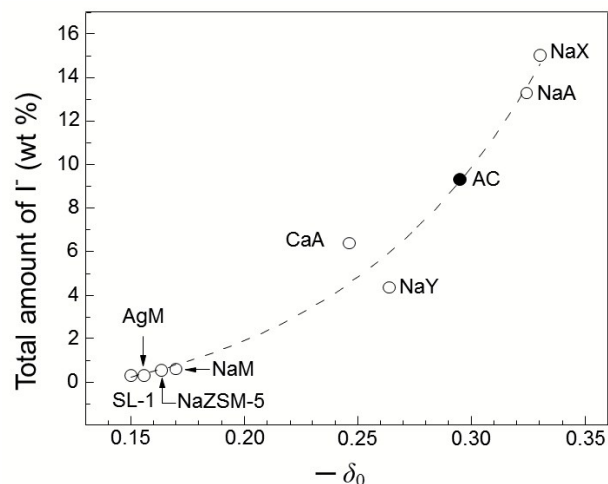


Fig. 5. The relationship between the total amount of I^- produced both in solution and in the adsorbent and the partial negative charge of the framework oxygen, $-\delta_o$

of I^- generated (Fig. 5). These results clearly show that electron rich frameworks serve as reducing agents for I_2 . Furthermore, including the formation of I^- , the total amounts of I_2 scavenged by HISL, Si-BEA, and AC from the neutral aqueous solutions are 0.53, 0.44 and 0.72 g/g, respectively (Fig. 3j).

A second criterion that must be met by materials used to remove residual amounts of I_2 from dissolver solutions is that they are inert in highly concentrated (>3 M) nitric acid

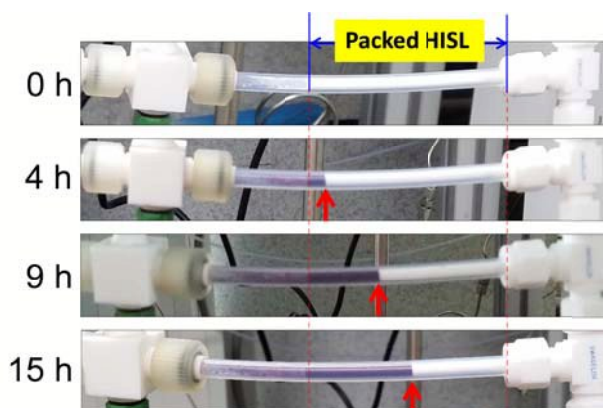


Fig. 4. The photographs taken after the periods of 0, 4, 9, and 15 h (as indicated) during the passage of the humid gas stream consisting of I_2 vapor and Ar through a Teflon tube packed with a HISL powder. The red arrows indicate the frontlines of I_2 -incorporating HISL.

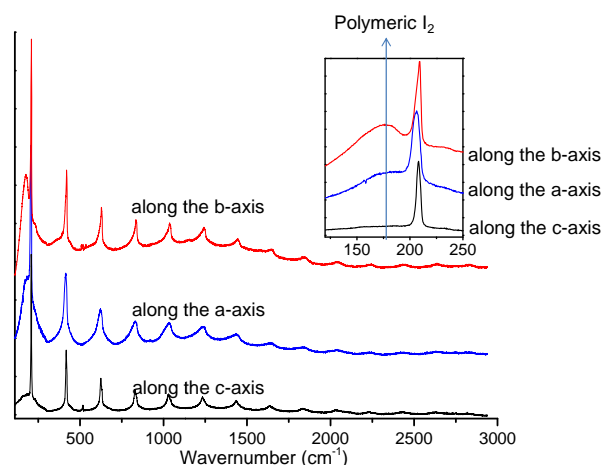


Fig. 6. The polarized micro Raman spectra of a single $12I_2@HISL$ crystal with the plane of incident excitation beam oriented parallel with the b , a , and c axes, respectively, as indicated. The inset shows the expanded spectra in the region between 125 and 250 nm.

solutions. We found that HISL and Si-BEA remain intact even after immersion in 5 M HNO_3 solution for 3 d. Furthermore, HISL and Si-BEA respectively capture 0.26 and 0.21 g/g of I_2 from a 5 M HNO_3 solution saturated with I_2 within 1 h. In contrast, AC captures only 0.04 g/g of I_2 under the same condition (Fig. 2k) and the electron rich materials such as ZIF-8, HKUST-1, NaX, NaA, AC, CaA, and NaY readily dissolve in aqueous HNO_3 even at concentrations as low as 0.1 M. The above results demonstrate the unparalleled superiority of all-silica zeolites, especially HISL, over AC as materials for directly removing I_2 from the dissolver solution.

The third criterion needed to be met by materials used to remove I_2 is that they are stable when exposed to γ , β , and α

radiation. It should be noted that zeolites have been widely used to capture radioactive Cs^+ and Sr^{2+} ions owing to the fact that they are stable to γ and β radiation. Clinoptilolite, a natural aluminosilicate zeolite, has been shown to possess Cs^+ and Sr^{2+} capturing abilities and that its abilities increase upon irradiation with a 8 MeV electron beam²⁰. HISL is a pure silica zeolite and, hence, it is expected (not experimentally tested) to be more stable than aluminosilicate zeolites under all radiation conditions. In contrast, carbon based materials such as AC, ZIF-8, and HKUST-1 are expected to be unstable when exposed to γ , β , and α radiation.

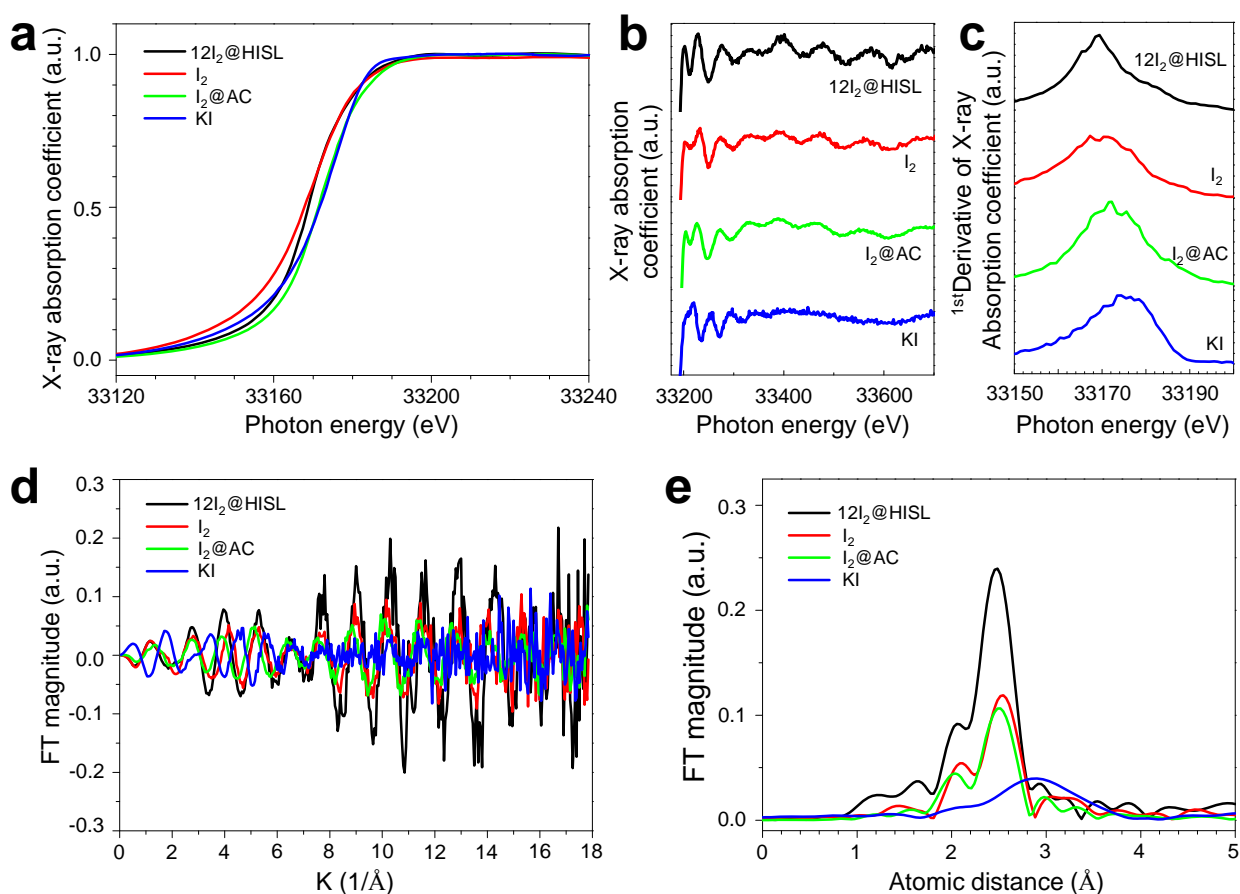


Fig. 7. Iodine K -edge X-ray absorption near edge structure spectra (XANES) (a), extended X-ray absorption fine structure (EXAFS) spectra (b), the plots of the 1st derivative of the x-ray absorption coefficient with respect to photon energy (c), the plots of the Fourier transform magnitude with respect to wave number (k) (d) and with respect to atomic distance (e) of the samples indicated in each panel.

Table 1 Crystal structure data of HISL and 12I₂@HISL at 150 and 296 K

	HISL		I ₂ @HISL	
	(150 K)	(296 K)	(150 K)	(296 K)
Crystal Syst.	Monoclinic	monoclinic	monoclinic	orthorhombic
Space Group	P2 ₁ /n	P2 ₁ /n	P2 ₁ /n	Pnma
a [Å]	13.347(3)	19.866(4)	13.354(3)	20.100(4)
b [Å]	20.082(4)	20.099(4)	20.087(4)	19.912(4)
c [Å]	19.827(4)	13.362(2)	19.868(4)	13.386(3)
β [°]	90.84(3)	90.48(3)	90.72(3)	90
V [Å ³]	5313.8(19)	5342.2(19)	5329.0(19)	5357.5(19)
σ [Mg/m ³]	1.803	1.793	2.747	2.732
Goof value F ²	1.135	1.340	1.037	1.027
R ₁	0.1199	0.1188	0.1294	0.0616
R _{1w}	0.3915	0.3651	0.3667	0.1559
*CCDC No.	1411127	910428	1411126	910429

I₂ desorption profiles of I₂-incorporated HISL, SL-1, Si-BEA, and AC (Fig. 3f) show that HISL and AC do not release I₂ at temperatures below 50 °C under a N₂ stream. This result shows that HISL strongly retains I₂ at room temperature and, thus, does not allow it to migrate from particle to particle (Fig. 4). At 175 °C, however, adsorbed I₂ undergoes complete desorption from HISL. In contrast, 35% (with respect to the total adsorbed amount) of iodine remains adsorbed in AC under this condition. Soaking I₂-incorporated HISL and SL-1 in organic solvents, such as ethanol, carbon tetrachloride (CCl₄) and *n*-hexane, leads to complete removal of I₂. However, I₂-incorporated AC retains 15% (with respect to the total adsorbed amount) of I₂ in the form of I⁻ when soaked in these solvents. Such a unique property of HISL can be utilized advantageously to facilitate desorption of I₂. For example, I₂ removed from this sorbent by extraction with ethanol can be transformed into insoluble AgI powder by treatment with AgNO₃ (eq. 3). Alternatively, I₂ in HISL can be desorbed using a hot (≥100 °C) air stream and the desorbed I₂ can be passed into an aqueous AgNO₃ solution. In this way, the volume of radioactive waste to be permanently sequestered can be minimized. It should be noted that the temperature required (100-175 °C) for this physical desorption process is much lower than that needed for chemical desorption (500 °C). Finally, charging of the fixed bed columns with HISL foams^{21,22} can be also utilized to avoid pressure drop during the passage of off gases and hot air.

Evidence for the existence of I₂ only in the neutral form in HISL

To prove that I₂ exists only in the neutral but not in the reduced form in HISL we obtained polarized micro Raman spectra of the fully I₂-incorporating HISL along the polarized excitation beam oscillating along the *a*-, *b*-, and *c*- directions (Fig. 6). They all showed the typical Raman spectra of I₂.²³⁻²⁵ If some of the incorporated I₂ is reduced within HISL, the produced I⁻ ion will form I₃⁻ with the unreduced I₂. It is well known that I₃⁻ shows a distinctive vibrational band at 110 cm⁻¹.²³⁻²⁵ However, none of the Raman spectra shown in Fig. 6 shows the existence of I₃⁻ band, clearly showing that all of the incorporated I₂ in HISL exist in the neutral form. It is also well known that a broad scattering appears at ~175 nm when I₂ forms a polymer.²³⁻²⁵ As shown more clearly in the inset of Fig. 6, the Raman spectra along the *a*- and *b*- axes show the presence of the broad ~175 nm band, more intensely along the *b*-axis. These results show the incorporated I₂ form polymeric I₂ along the *a* and *b* axes, to a larger degree along the *b*-axis. The absence of the ~175 nm band along the *c*-axis indicates that the incorporated I₂ does not form polymeric I₂ along the axis.

We also obtained iodine *K*-edge X-ray absorption near edge structure spectra (XANES) (Fig. 7a), extended X-ray absorption fine structure (EXAFS) spectra (Fig. 7b), the plots of the 1st derivative of the x-ray absorption coefficient with respect to photon energy (Fig. 7c), the plots of the Fourier transform magnitude with respect to wave number (*k*) (Fig. 7d) and with respect to atomic distance (Fig. 7e) of 12 I₂-incorporated HISL (12I₂@HISL), fully I₂-incorporated AC (I₂@AC), and solid I₂, and KI. The comparison of the data set shown in Fig. 7b-d shows that the data set of 12I₂@HISL matches very well with that of I₂ but not with that of KI, confirming that the iodine molecules incorporated in HISL

indeed exist in the neutral but not in the reduced form. From Fig. 7e we obtained that that average I-I-distance of the iodine molecules in $12\text{I}_2@\text{HISL}$ is 2.682 (1) Å.

Supramolecular structures of I_2 molecules in HISL

We determined crystal structures of both HISL and the HISL- I_2 complex ($12\text{I}_2@\text{HISL}$) at 298 K and at 150 K, respectively, by using single-crystal X-ray diffraction with synchrotron radiation ($\lambda = 0.6700$ Å). Analysis of the structures shows that, upon adsorption of I_2 , the unit cell parameters of HISL change slightly from those of monoclinic to orthorhombic lattice systems at 296 K and the calculated densities increase

from 1.796 to 2.732 Mg/m^3 . At 150 K the lattice system changes back to monoclinic with the calculated density of 2.747 Mg/m^3 . The unit cell compositions are $\text{Si}_{96}\text{O}_{192}$ and $\text{I}_{24}\text{Si}_{96}\text{O}_{192}$, respectively. Thus, these observations demonstrate that HISL accommodates up to 12 I_2 molecules per unit cell, which corresponds to 53.8% of the HISL host by weight or 0.538 g per g of HISL. This value well matches the experimentally determined, maximum amount of I_2 adsorbed from a stream of I_2 vapour (Fig. 3a,b) and from an aqueous solution (Fig. 3j).

Further analysis of the crystal structure of $12\text{I}_2@\text{HISL}$

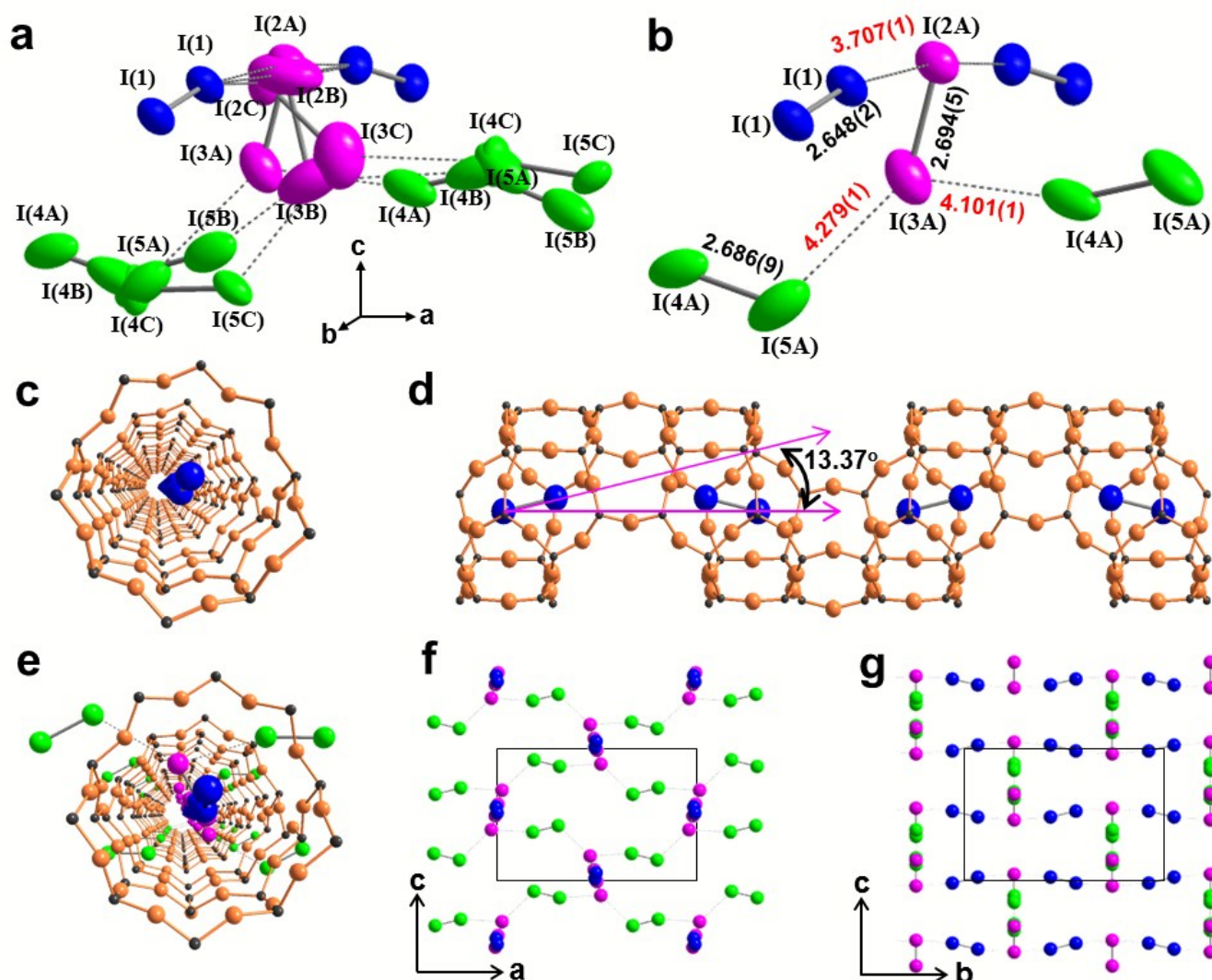


Fig. 8 The disordered 3D networking structure of the iodine molecules in HISL shown with the thermal ellipsoids drawn at the 50% probability level (a). The structure A with the highest occupancy at room temperature with the displacement ellipsoids at 50% probability (b). A perspective projection of the straight b -channel with the I_2 molecules oriented parallel to the b -axis (c) and its side view showing the tilted angle of I_2 molecule with respect to the b -axis (d). A perspective view of the straight b -channel incorporating all three types of I_2 molecules (e). 3D network of I_2 molecules, viewed along the b -axis (f) and a -axis (g).

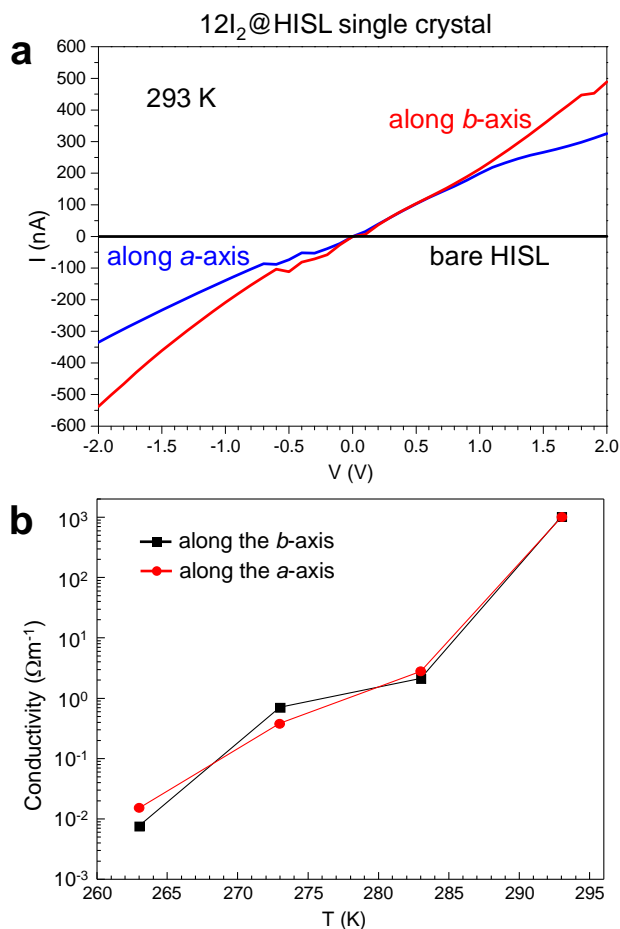


Fig. 9. I-V plots of 12I₂@HISL along the a- and b-axes and bare HISL at 293 K (a) and the plots of the conductivities of 12I₂@HISL along a- and b-axes with respect to temperature (b).

shows that five independent iodine atoms are located in the unit cell. Four I₂ molecules exist in *b*-channels [labelled as I(1)-I(1)], four exist at the channel intersections [labelled as I(2)-I(3)], and four exist in *a*-channels [labelled as I(4)-I(5)] (Fig. 8a). Inspection of the electron density map of 12I₂@HISL reveals that I(2), I(3), I(4), and I(5) are severely disordered. A combination of three model structures with different occupancies of the I₂ molecules was employed to resolve the disorder of the iodine atoms during refinement. The first combination (A, B, and C) with the respective occupancies of 47.03, 30.34 and 22.63% was employed to clarify the structure at 296 K. The second combination (A', B' and C'), with the respective occupancies of 40.02, 30.76, and 29.22%, was used to clarify the structure at 150 K. The crystal structural data are summarized in Table 1.

Structure A of 12I₂@HISL is shown in Fig. 8b together with their intra and intermolecular structures. The I(1)-I(1) bond length is 2.648(2) Å and those of I(2A)-I(3A) and I(4A)-I(5A) are 2.693(5) and 2.701(9) Å, respectively. The intermolecular distances between I(1)⋯I(2A), I(3A)⋯I(4A), and I(3A)⋯I(5A) are 3.707(1), 4.101(1), and 4.279(1) Å, respectively. The average I(2)-I(3) and I(4)-I(5) bond lengths are 2.693 and 2.701 Å, respectively, and the average intermolecular distances between I(1)⋯I(2), I(3)⋯I(4), and I(3)⋯I(5) are 3.703, 4.363, and 4.061 Å, respectively. The average bond length of I₂ in the three disordered structures is 2.681 Å, a value that matches well the I₂ bond length determined by EXAFS [2.682(1) Å].

Of particular interest is the finding that the I(1)-I(1) bond length [2.648(2) Å] in 12I₂@HISL is the shortest ever observed for neutral I₂ in various media (2.681-2.720 Å) under the ambient conditions (Supplementary Table S13)²⁶. However, this bond length is still longer than that of I₂⁺ (2.56 Å)²⁷. This observation suggests that the *b*-oriented HISL channel causes intercalated I₂ to exist in a compressed state. The average intermolecular distance between I(1)⋯I(2A) (3.707 Å) is also shorter than that in crystalline I₂ (3.972-4.412 Å) at room temperature but it is in the range of the I⋯I distance in crystalline I₂ at -173 °C and 1 bar²⁴ (3.496-4.412 Å) or at room temperature at 206 kbar (2.960-3.730 Å)²⁸. In fact, as the pressure on crystalline I₂ increases the I-I bond length increases while the intermolecular I⋯I distance decreases as a consequence of the occurrence of a phase transition from the molecular to atomic crystals²⁸⁻³⁰. For instance, the I-I bond length at 206 kbar is 2.78²⁸. However, it is unique that, unlike in iodine crystals, I₂ molecules located along the *b* and *c* axes in 12I₂@HISL have compressed bond lengths and intermolecular distances. The I(1)-I(1) molecules in the array viewed along the *b*- and *a*-channels (Fig. 8c and Fig. 8d, respectively) are tilted by up to 13.37° toward the intersection with respect to the *b*-axis.

The average bond lengths of I(2)-I(3) and I(4)-I(5) (2.693 and 2.701 Å, respectively) obtained from analysis of structures A, B, and C are also shorter than that of solid I₂ (2.720 Å at room temperature)²⁶. However, the average intermolecular distances between I(3)⋯I(5) and I(3)⋯I(4) (4.059 and 4.413 Å) are in the range of those observed for solid I₂ under ambient conditions^{28,29}. Thus, the I-I bond lengths in I₂ molecules located along the *a* and *c* axes in 12I₂@HISL are compressed while the intermolecular distances remain unchanged, a phenomenon not observed in crystalline I₂.

A perspective view of the three types of I₂ molecules incorporated within a straight channel in 12I₂@HISL is shown in Fig. 8e and the three-dimensional (3D) networking of I₂ molecules in structure A is shown in Figs. 8f and 8g, respectively. The absence of intermolecular I...I interaction along the c axis coincides well with the lack of the ~175 cm⁻¹ peak along the c axis observed from the polarized micro Raman spectrum of a single crystal of 12I₂@HISL. Significantly, this is the first observation of the formation of a unique 3D supramolecular network of neutral I₂ molecules in a zeolite. Upon decreasing the temperature from 296 K to 150 K, the average I₂ bond distance decreases from 2.681 to 2.651 Å and the intermolecular I...I distance along the b-axis decreases from 3.703 to 3.684 Å, while that along the a-axis remains the same at 4.212 Å. Thus, as the temperature decreases the incorporated molecules undergo greater compression along the b-axis.

Very high conductivities of 12I₂@HISL

The experimentally measured conductivities of 12I₂@HISL at 293 K along the *a* and *b* axes, determined by using electric force microscopy (EFM), are 1.7×10^4 and 2.0×10^4 S m⁻¹, respectively (Fig. 9a), while those of unloaded HISL are 3.25×10^{-1} and 1.25×10^{-1} S m⁻¹. The conductivities of 12I₂@HISL, measured by using the two-probe method, are also ca. 1×10^3 S m⁻¹ at 293 K. Thus, the conductivity of 12I₂@HISL under ambient conditions is at least 8 orders of magnitude larger than that of crystalline I₂ ($2 \times 10^{-7} \sim 5 \times 10^{-5}$ S m⁻¹)³¹ and comparable with that of graphite ($3.3 \times 10^2 \sim 3 \times 10^5$ S m⁻¹). The nature of the conductivity displayed by 12I₂@HISL is semiconductivity because it sharply decreases with decreasing temperature, becoming near 0 S m⁻¹ at 263 K (Fig. 9b). Thus, the conductivity of 12I₂@HISL is comparable to that of solid I₂^{32,33} at 184 kbar. In this respect, it is quite interesting that 12I₂@HISL displays very high conductivity even under ambient conditions where the I-I and bond lengths and I...I intermolecular distances are markedly shorter than those of solid I₂.

It was shown earlier that the conductivities of I₂-incorporated and I₂-treated MOFs,³⁴⁻³⁸ range between 10⁻⁸ and 10⁻¹ S m⁻¹. These values are much smaller than that of 12I₂@HISL. Furthermore, the nature of the conductivities of I₂-incorporated and I₂-treated MOFs are different from that of 12I₂@HISL because, in the former case, the oxidized MOF frameworks and the produced I⁻ also contribute to the overall conductivity³⁴⁻³⁸. The above results show that 12I₂@HISL is a promising semiconducting material with tuneable *E_g* values that has the potential of being utilized in novel optoelectronic functional devices³⁹⁻⁴¹.

The total density of states (TDOS) of HISL and 12I₂@HISL and the partial density of state (PDOS) for I in

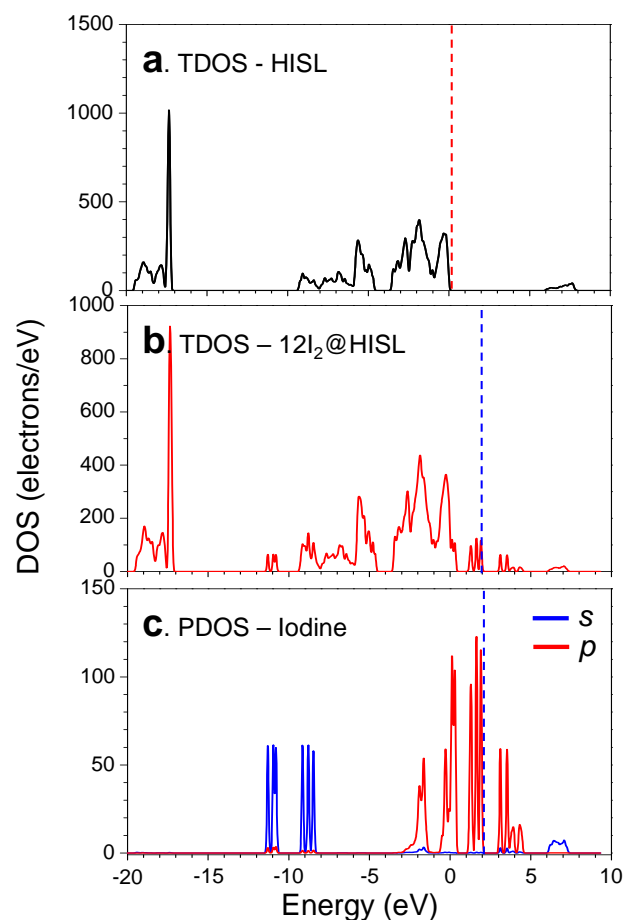


Fig. 10. Calculated total densities of states (TDOS) of HISL (a) and 12I₂@HISL of model A (b), and partial density of states (PDOS) of iodine in 12I₂@HISL of model A (c).

12I₂@HISL, calculated using CASTEP, are shown in Fig. 10 for the structure A. Ongoing from HISL to 12I₂@HISL the Fermi level shifts to higher energy by 1.94 eV. The calculated average band gap energy based analysis of the combination of the three I₂ structures (*E_g*) is 1.044 eV. The purely theoretical band gap energy, obtained after energy minimization of the structure and without any structural restrictions, is 0.895 eV. Thus, the results of the theoretical treatment support the semiconductor behavior of 12I₂@HISL and provides information about the origin of its semiconductor property.

Conclusions

All-silica zeolites, especially HISL, demonstrate the unparalleled superiority over AC, aluminosilicate zeolites, and metal organic framework (MOF) as materials for removal of radioactive I₂ and RI from the stream of humid, acidic, and oxidizing off gas and directly removing radioactive I₂ from

the highly acidic dissolver solution. However, they are not suitable as HI removers.

The unparalleled I₂ sorbent property of HISL is concluded to be associated with its very high hydrophobicity arising from its very small number of framework defects, its unique ability to tightly fit I₂ within the channels, and its ability to form of a semiconducting three-dimensional supramolecular network of I₂. In the crystalline form of the HISL-12I₂ complex, (12I₂@HISL) the average I-I bond distance (2.681 Å) is much shorter than that in crystalline solid I₂ at room temperature (2.720 Å). In contrast to solid I₂ under ambient conditions, both the intramolecular I-I and intermolecular I...I bonds in 12I₂@HISL are compressed along the b-axis and only the intramolecular I-I bond is compressed along the a-axis. The conductivity of 12I₂@HISL at room temperature is in the range of $1.7\text{--}2.0 \times 10^4 \text{ S m}^{-1}$, a value that is at least eight-orders of magnitude larger than that of crystalline I₂ under ambient conditions. Finally, the results of CASTEP calculations confirm and help explain the source of the semiconductor behaviour of 12I₂@HISL.

Methods

Materials

Aqueous tetraethyl ammonium hydroxide (TEAOH, 35%, Alfa), aqueous tetrapropyl ammonium hydroxide (TPAOH, 1M, Sigma-Aldrich), ammonium hexafluoro silicate [(NH₄)₂SiF₆, 98 %, Sigma-Aldrich], tetraethylorthosilicate (TEOS, 98 %, Acros-Organic), methyl iodide and ethyl iodide (99.5%, Acros-Organic), activated carbon (Sigma-Aldrich) were purchased and used as received. Iodine (I₂, 99 %, Samchun Pure Chemical Co.Ltd) was purified by sublimation before use. Methyl iodide (99%) and ethyl iodide (99%) were purchased from Acros Organics and used as received. LTA (Si/Al = 1.0) (4A, Lot No. 941089060329) was purchased from Union Carbide. FAU (Si/Al = 1.0, zeolite X) (13X, Lot No. 943196110142) and FAU (Si/Al = 2.6, zeolite Y) (LZY-52, Lot No. 968087061020-S) were purchased from Strem and Union Carbide, respectively. MOR (8.2) (EZ-320 P, code 29829) is the sample purchased from England Corporation Catalyst for Industry. bis-N,N-(tripropylammonium-hexamethylene) di-N,N-propylammonium trihydroxide (trimer-TPAOH) was synthesized according to the reported procedure⁴¹. ZIF-8 (Basolite™ Z1200-Sigma-Aldrich) and HKUST-1 (Basolite® C300-Sigma-Aldrich) were purchased and used as received. ZnSacc was synthesized according to the known procedure¹⁶ with some modifications.

Preparation of SL-1 crystals

Rounded coffin-shaped SL-1 crystals with the average size of $1.5 \times 0.6 \times 1.9 \mu\text{m}^3$ were synthesized from a gel composed of

TEOS, TPAOH, and H₂O with the mole ratio of 6:0.9:620. The above synthesis gels were prepared by introducing TEOS into the solution containing TPAOH and H₂O. The mixture transformed into a clear gel after stirring for 24 h at room temperature. The clear gel was filtered through a filter paper (Whatman® No.5) and charged into a Teflon-lined autoclave. The hydrothermal reaction was carried out at 150 °C for 12 h with vigorous stirring with the aid of a magnetic stirrer. The obtained crystals were thoroughly washed with copious amounts of DDW to remove the mother liquor and dried at 100 °C by placing them in an oven overnight. To remove organic template, these crystals were calcined at 550 °C for 16 h under oxygen flow.

Preparation of HISL crystals

HISL was prepared by secondary growth using the gel consisting of TEOS, TEAOH, (NH₄)₂SiF₆, and H₂O using SL-1 crystals as seed crystals. The gel with molar ratio of TEOS, TEAOH, (NH₄)₂SiF₆, and H₂O was 4.00:1.92:0.36:50 and was prepared as follows. (I) Preparation of the TEOS/TEAOH solution (Solution I): TEAOH (35 %, 13.4 g) and distilled deionized water (6.3 g) were sequentially added into a plastic beaker containing 21.2 g of TEOS (98 %). This beaker containing the above solution was tightly covered using plastic wrap and magnetically stirred for about 30 min until the solution became clear. The above calcined SL-1 powder (0.24 g) was added and stirred additionally for 10 min. (II) Preparation of the TEAOH/(NH₄)₂SiF₆ solution (Solution II): TEAOH (35 %, 6.7 g), (NH₄)₂SiF₆ (1.64 g), and distilled deionized water (3.15 g) were introduced into a plastic beaker and stirred until all (NH₄)₂SiF₆ became dissolved. Solution II was quickly poured into Solution I with vigorously stirring. The mixture solidified immediately. The solidified mixture was stirred for additional 2 min using a plastic rod, and aged under a static condition for 6 h. After aging, the semisolid gel was ground using a food mixer and transferred into a Teflon-lined autoclave. The sealed autoclaves were placed in an oven preheated at 165 °C. After 7 days, the autoclaves were removed from the oven and quickly cooled by running tap water onto them. The solid product was collected, washed with copious amount of distilled deionized water and dried at 100 °C by placing them in an oven overnight. The obtained SL-1F was calcined at 550 °C for 16 h under oxygen flow.

Preparation of large HISL crystals having flat (100) faces for conductivity measurements

Leaflet shaped SL-1 crystals were first prepared according to the reported procedure using *trimer*-TPAOH as the structure directing agent^{42,43}. Large SL-1F crystals having flat (100) faces were prepared by secondary growth of the leaflet shaped SL-1 crystals in a gel prepared to produce HISL.

Preparation of HISL single crystals

HISL single crystals with the average size of $20 \times 15 \times 50 \mu\text{m}^3$ were synthesized from a gel composed of fumed silica, TEAOH, KOH, NH_4F and H_2O using pure silica beta zeolite (Si-BEA) with particle size of $34 \times 35 \times 50 \mu\text{m}^3$ as additional seed. The above gel with the mole ratio of 1:0.3:0.1:0.18:15 was prepared as follows:

(I) In a plastic beaker containing TEAOH (35 %, 16.62 g), KOH (95 %, 0.60 g) was added and subsequently dissolved with the help of a magnetic stirrer. Fumed silica (6.0 g) was added into the above TEAOH/KOH solution and stirred until it turned into a clear and viscous gel. DDW (10 g) was added. Finally, Si-BEA powder (200 mg) was added and the mixture was stirred for about 10 min.

(II) Independently, a plastic beaker containing a clear solution of TEAOH (35 %, 7.57 g), NH_4F (0.67 g) and DDW (3.87 g) was prepared.

Solution (II) was poured into solution (I) with vigorously stirring. The gel was kept stirring at room temperature for 18 h. After aging, the viscous gel was transferred into a Teflon-lined autoclave. The sealed autoclaves were placed in an oven preheated at 165 °C. After 12 days, the autoclaves were removed from the oven and quickly cooled by running tap water onto them. The solid product was collected, washed with copious amounts of DDW and dried at 100 °C by placing them in an oven overnight. The obtained SL-1F single crystals were calcined at 550 °C for 36 h under an oxygen flow. The temperature was slowly increased from the room temperature to 550 °C during 18 h and stayed at the temperature for 36 h slowly cooled to room temperature during the period of 12 h.

Preparation of Si-BEA crystals

Si-BEA was prepared from a gel consisting of fumed silica, TEAOH, $(\text{NH}_4)_2\text{SiF}_6$, KOH and H_2O by adopting the literature procedure⁴³. The molar ratio of the components in the gel was 4.00:1.92:0.36:0.40:31.20. The hydrothermal reaction was carried out at 165 °C. After 7 days of reaction, the autoclave was removed from the oven and quickly cooled to room temperature by running tap water onto them. The obtained crystals were thoroughly washed with copious amounts of distilled deionized water and dried at 100 °C by placing them in an oven overnight.

Adsorption of I_2 from the vapour phase

An adsorption set up consisting of a water bubbler, a tube containing solid I_2 , a Teflon sorption tube, and a tube containing an aqueous $\text{Na}_2\text{S}_2\text{O}_3$ solution was prepared and Ar (2 mL/min) was passed through the set up. A nitric acid solution (5 M) was introduced into the water bubbler to allow

the carrier gas to carry the vapours of nitric acid as well as moisture before the carrier gas to enter the I_2 -containing tube. The carrier gas was also bypassed directly to the I_2 -containing tube to allow the carrier gas to carry dry I_2 vapour into the adsorption tube. The aqueous $\text{Na}_2\text{S}_2\text{O}_3$ solution was to trap I_2 vapour.

Adsorption of I_2 from the aqueous solution

An aliquot (100 mL) of the I_2 solution (0.25 g per 100 mL) was added into a glass vial containing 500 mg of a solid adsorbent. The mixture was shaken for 1 min or magnetically stirred for 1 h. The heterogeneous solution was then centrifuged and the concentration of the supernatant solution was measured by titration with a $\text{Na}_2\text{S}_2\text{O}_3$ solution.

Adsorption of methyl iodide and ethyl iodide

An online set up consisting of a water bubbler, a tube containing methyl iodide or ethyl iodide, a Teflon sorption tube, a tube containing a NaOH solution, and a GC equipped with a flame ionization detector (FID) was prepared and Ar (2 mL/min) was passed through the set up. A nitric acid solution (5 M) was introduced into the bubbler tube instead of distilled water to allow the carrier gas to carry the vapours of nitric acid as well as moisture before the carrier gas to enter the I_2 -containing tube. The carrier gas was also bypassed directly to the methyl iodide or ethyl iodide-containing tube to allow the carrier gas to carry dry methyl iodide or ethyl iodide vapour into the adsorption tube. The aqueous NaOH solution was to trap the vapours coming from nitric acid.

X-ray absorption measurements

Iodine K-edge X-ray absorption spectra, X-ray absorption near edge structure (XANES), and extended X-ray absorption fine structure (EXAFS), were collected on BL10C beam line at the Pohang light source (PLS-II) with a ring current of 125 mA at 3.0 GeV. The monochromatic X-ray beam could be obtained from high intense X-ray photons of multipole wiggler source using liquid-nitrogen cooled Si (111) double crystal monochromator (Bruker ASC). The X-ray absorption spectroscopic data were recorded for the uniformly dispersed powder samples with a proper thickness on the polyimide film, in fluorescence mode with PIPS detector. Higher order harmonic contaminations were eliminated by detuning to reduce the incident X-ray intensity by ~20%. Energy calibration has been simultaneously carried out for each measurement with reference iodine molecule powder placed in front of the third ion chamber. The data reductions of the experimental spectra to normalized XANES and Fourier-transformed radial distribution function (RDF) were performed through the standard EXAFS procedure.

X-ray crystallographic analysis.

Collection of single crystal x-ray diffraction

The diffraction data were obtained from single crystals (~10.0 x 10.0 x 5.0 μm^3) of HISL and $12\text{I}_2@$ HISL using a ADSC Quantum 210 CCD diffractometer located in Macromolecular Crystallography Wiggler Beamline 2D in Pohang Accelerator Laboratory (PAL). Both diffraction data were collected by the using synchrotron radiation ($\lambda = 0.6700$ and 0.7000 Å) with the exposed time of 2 sec per frame and total 360 frames using ADSC Q210 ADX program⁴⁴ that are rotated by the scan width of 1.00° in ω angle at 150 K and 296 K, respectively. Both crystal data were collected to primitive triclinic lattice system (space group P1) for a full set data, and then were processed and scaled by using HKL3000.⁴⁵ The matched Bravais lattice systems were concluded to be the monoclinic and orthorhombic lattice systems by autoindexing of the collected diffraction peaks.

Crystal Structure Refinements

The crystal structures of HISL and $12\text{I}_2@$ HISL were solved by the direct method with SHELXTL-XS program and refined by full-matrix least-squares calculations with SHELXTL-XL (Ver. 2008) program package.⁴⁶ In the structure refinements, the chemical elements were modified using the instruction of DISP (the dispersion and the absorption coefficient of particular elements) at the wavelength 0.6700 (296 K) and 0.7000 Å (150 K). The crystal structures of HISL and $12\text{I}_2@$ HISL were solved in two different space groups: (i) HISL; centrosymmetric monoclinic ($P2_1/a$) at 150K and 296 K. (ii) $12\text{I}_2@$ HISL; monoclinic ($P2_1/a$) at 150 K and orthorhombic ($Pnma$) at 296 K. The crystal structural data can be obtained free of charge from the Cambridge Crystallographic Data Centre via www.ccdc.cam.ac.uk/data_request/cif.

Acknowledgements

This investigation was financially supported by the Korea Centre for Artificial Photosynthesis, located at Sogang University and the Ministry of Education of Science and Technology through the National Research Foundation of Korea, No. 2009-0093886. X-ray crystallographic data were collected using a synchrotron radiation beamline (PLS-II 2D-SMC) at Pohang Accelerator Laboratory, Korea. We thank Dr. Min-Gyu Kim (10C Wide Energy XAFS) and Dr. Nark Eon Sung (8C Nanoprobe XAFS) at the Pohang Accelerator Laboratory, Korea for their great help to measure and analyse the EXAFS data. We also thank J. Y. Lee for help in creating Fig. 1. Sogang University has filed patents on the results presented here.

References

1. D. R. Haefner, T. J. Tranter, *Methods of gas phase capture of iodine from fuel reprocessing off-gas: a literature survey*, INL/EXT-07-12299, (Idaho National Laboratory: Idaho Falls, ID, 2007).
2. B. Clément, L. Cantrel, G. Ducros, F. Funke, L. Herranz, A. Rydl, G. Weber, C. Wren, *State of the art report on iodine chemistry*, NEA/CSNI/R(2007)1, 2007, 1-60.
3. *Treatment, conditioning and disposal of iodine-129*, Technical Report Series No. 276, (IAEA, Vienna, 1987).
4. K. W. Chapman, P. J. Chupas, T. M. Nenoff, *J. Am. Chem. Soc.*, 2010, **132**, 8897-8899.
5. J. S. Hoskins, T. Karanfil, S. M. Serkiz, *Environ. Sci. Technol.* 2002, **36**, 784-789.
6. M. V. Wilkinson, A. V. Mondino, A. C. Manzini, *J. Radioanal. Nucl. Chem.*, 2003, **256**, 413-415.
7. W. Colcleugh, E. A. Moelwyn-Hughes, *J. Chem. Soc.* 1964, 2542-2545.
8. M. K. Song, E. Y. Choi, Y. Kim, *J. Phys. Chem. B*, 2003, **107**, 10709-10714.
9. S. D. Fava, T. J. Garino, T. M. Nenoff, *Ind. Eng. Chem. Res.*, 2012, **51**, 614-620.
10. K. W. Chapman, D. F. Sava, G. J. Halder, P. J. Chupas, Nenoff, *J. Am. Chem. Soc.* 2011, **133**, 18583-18585.
11. D. F. Sava, M. K. Rodriguez, K. W. Chapman, P. J. Chupas, J. A. Greathouse, P. S. Crozier, T. M. Nenoff, *J. Am. Chem. Soc.*, 2011, **133**, 12398-12401.
12. M.-H. Zeng, Q. X. Wang, Y. X. Tan, S. Hu, H. X. Zhao, L. S. Long, M. Kurmoo, *J. Am. Chem. Soc.* 2010, **132**, 2561-2563.
13. J.-P. Lang, Q.-F. Xu, R.-X. Yuan, B. F. Abrahams, *Angew. Chem. Int. Ed.* 2004, **43**, 4741-4745.
14. K. S. Park, Z. Ni, A. P. Cote, A. P. Cote, J. Y. Choi, R. Huang, F. J. Uribe-Romo, H. K. Chae, M. O'Keeffe, O. M. Yaghi, *PNAS* 2006, **103**, 10186-10191.
15. S. S.-Y. Chui, S. M.-F. Lo, J. P. H. Charmant, A. G. Orpen, I. D. Williams, *Science*, 1999, **283**, 1148-1150.
16. B. F. Abrahams, M. Moylan, S. D. Orchard, R. Robson, *Angew. Chem. Int. Ed.* 2003, **42**, 1848-1851.
17. P. Cautlet, J.-L. Paillaud, A. Simon-Masseron, M. Soulard, J. Patarin, *C. R. Chimie*, 2005, **8**, 245-266.
18. O. Larlus, V. Valtchev, *Micropor. Mesopor. Mater.*, 2006, **93**, 55-61.
19. R. T. Sanderson, *Chemical Bonds and Bond Energy* (Academic Press, New York 1976).
20. H. Yeritsyan, A. Sahakyan, V. Harutyunyan, S. Nikoghosyan, E. Hakhverdyan, N. Grigoryan, A. Hovhannisyanyan, V. Atoyan, Y. Keheyanyan, C. Rhodes, *Scientific Reports*, 2013, **3**, 1-7.
21. Y.-J. Lee, J. S. Lee, Y. S. Park, K. B. Yoon, *Adv. Mater.*, 2001, **13**, 1259-1263.
22. Y.-J. Lee, K. B. Yoon, *Micropor. Mesopor. Mater.*, 2006, **88**, 176-186.
23. U. Buontempo, A. D. Cicco, A. Filippini, M. Nardone, P. Postorino, *J. Chem. Phys.* 1997, **107**, 5720-5726.
24. C. G. Davies, R. J. Gillespie, P. R. Ireland, J. M. Sowa, *Can. J. Chem.* 1974, **52**, 2048-2052.
25. O. Shimomura, K. Takemura, Y. Fujii, S. Minomura, *Phys. Rev. B*, 1978, **18**, 715-719.

26. K. Takemura, S. Minomura, O. Shimomura, Y. Fujii, J. D. Axe, *Phys. Rev. B*, 1982, **26**, 998-1004.
27. T. Kenichi, S. Kyoko, F. Hiroshi, O. Mitsuko, *Nature*, 2003, **423**, 971-974.
28. J. T. Ye, Z. K. Tang, G. G. Siu, *Appl. Phys. Lett.*, 2006, **88**, 073114.
29. J. P. Zhai, H. F. Lee, I. L. Li, S. C. Ruan, Z. K. Tang, *Nanotechnology*, 2008, **19**, 175604.
30. A. Basch, M. Hartl, P. Behrens, *Micropor. Mesopor. Mater.*, 2007, **99**, 244-250.
31. J. S. Ham, *J. Polym. Sci. C.*, 1967, **17**, 225-232.
32. A. S. Balchan, H. G. Drickamer, *J. Chem. Phys.*, 1961, **34**, 1948-1949.
33. B.M. Riggleman, H.G. Drickamer, *J. Chem. Soc.*, 1963, **38**, 2721-2724.
34. Y. Lin, W. Massa, S. Dehnen, *J. Am. Chem. Soc.*, 2012, **134**, 4497-4500.
35. T. Hasell, M. Schmidtman, A. I., *J. Am. Chem. Soc.*, 2011, **133**, 14920-14923.
36. Z. Yin, W Q.-X. ang, M.-H. Zeng, *J. Am. Chem. Soc.*, 2012, **134**, 4857-4863.
37. T. Hertzsch, F. Budde, E. Weber, J. Hulliger, *Angew. Chem. Int. Ed.* 2002, **41**, 2281-2284.
38. Y. Kobayashi, B. Jacobs, M. D. Allendorf, J. R. Long, *Chem. Mater.* 2010, **22**, 4120-4122.
39. J. Ye, L. S. Ma, J. L. Hall, *Phys. Rev. Lett.*, 2001, **87**, 270801.
40. W. Guo, D. Wang, J. Hu, Z. K. Tang, S. Du, *Appl. Phys. Lett.*, 2011, **98**, 043105.
41. K. Hosaka, H. Shimada, H. Chiba, H. Katsuki, Y. Teranishi, Y. Ohtsuki, K. Ohmori, *Phys. Rev. Lett.*, 2010, **104**, 180501.
42. Z. P. Lai, M. Tsapatsis, J. R., *Adv. Funct. Mater.*, 2004, **4**, 716-729.
43. C. T. T. Pham, H. S. Kim, K. B. Yoon, *Science*, 2011, **334**, 1533-1538.
44. A. J. Arvai, C. Nielsen, *ADSC Quantum-210 ADX Program* (Area Detector System Corporation; Poway, CA, USA 1983).
45. Z. Otwinowski, W. Minor, in *Methods in Enzymology* (ed. Carter, Jr., C. W.; Sweet, R. M. Academic Press, New York, vol. 276, part A, pp. 307, 1997).
46. G. M. Sheldrick, SHELXTL-PLUS, *Crystal Structure Analysis Package*, Bruker Analytical X-Ray, (Madison, WI, USA, 1997).